This article has been accepted for publication in a future issue of this journal, but has not been fully edited. Content may change prior to final publication. Citation information: DOI 10.1109/TPEL.2015.2421480, IEEE Transactions on Power Electronics

Unity Power Factor Operation of Indirect Matrix Converter Tied to Unbalanced Grid

Mahmoud Hamouda, Handy Fortin Blanchette, *Member, IEEE*, and Kamal Al-Haddad, *Fellow, IEEE*

***Abstract*— This paper presents a new control method for Indirect Matrix Converter operating under unbalanced grid voltages. The proposed method aims to achieve balanced output voltages as well as a near unity input power factor operation. First, an opportune reference current accurately generated, and a proportional integral resonant controller are designed in a dq reference frame that is synchronized with the positive sequence of the grid voltages so as to achieve a perfect tracking of input reactive power reference. Then, a real-time estimator of the virtual dc-link voltage is developed with the aim to provide balanced output voltages; therefore an almost constant active power free of low frequency ripple is supplied from the grid. Experimental results are presented to verify the feasibility and effectiveness of the proposed control method.**

***Index Terms*— matrix converters, resonant controllers, space vector modulation (SVPWM), unbalanced grid voltages, power factor correction, active rectifier, grid-tied converter**

NOMENCLATURE

d_a, d_b, d_c	Duty cycles applied to estimate the dc-link voltage.
d_{1I}, d_{2I}	Duty cycles applied to synthesize the output voltage space vector.
d_{1R}, d_{2R}	Duty cycles applied to synthesize the input current space vector's direction.
$E_{a,b,c}$	Instantaneous grid voltages in abc frame.
$\bar{E}$	Grid voltage space vector.
$\bar{E}^*$	Conjugate of $\bar{E}$.
$\bar{E}^+$	(+) sequence of grid voltage space vector.
E^+, E^-	Peak value of E_{abc} (+) and (-) sequences.
E_d^+, E_q^+	d-q components of (+) sequence of grid voltages expressed in the positive synchronous frame.
E_d^-, E_q^-	d-q components of (-) sequence of grid voltages expressed in the positive synchronous frame.
$E'_{a,b,c}$	Lagging orthogonal voltages of $E_{a,b,c}$.
$\bar{E}_\perp$	A space vector equivalent to $E'_{a,b,c}$.
$E_{d,q}$	d-q components of $E_{a,b,c}$.
$i_{ma,mb,mc}$	Instantaneous input currents in abc frame.
$\bar{I}_m$	Input current space vector.
$i_{a,b,c}$	Instantaneous line currents in abc frame.
$\bar{I}$	Line current space vector.
$\bar{I}^*$	Conjugate of $\bar{I}$.
I^+, I^-	Peak value of (+) and (-) sequences of $i_{a,b,c}$.
I_d^+, I_q^+	d-q components of line currents (+) sequence.
I_d^-, I_q^-	d-q components of line currents (-) sequence.
$i_{d,q}$	d-q components of $i_{a,b,c}$.
$i_{md,mq}$	d-q components of input currents $i_{ma,mb,mc}$.
K_i	The sector's number where $\bar{I}_m$ is lying.
K_{IR}	Gain of resonant term.
K_P, K_I	Proportional and integral gains of the PI controller.
K_{damp}	Damping gain of resonant term.
L, c, r	Input filter's inductance, capacitance, and resistance.
P^{in}	Instantaneous input active power.
Q_{damp}	Quality factor of resonant term.
Q_f	Quality factor of the input filter.
Q^{in}	Grid converter exchanged reactive power.
$Q^{in}_{0\_ref}$	Average reactive power reference.
s	Laplace variable.
$\langle \bar{S}_G \rangle_{T_c}$	Averaged switching function of the grid side converter.
T_c	Switching period.
$\langle V_{dc} \rangle_{T_c}$	Estimated average value of the dc-link voltage.
$V_{ma,mb,mc}$	Voltages across the input filter capacitors.
V_{md}	Direct component of $V_{ma,mb,mc}$.
φ^+, φ^-	Initial phase angles of (+) and (-) negative sequences of line currents.
φ_i	Phase angle between $\bar{E}^+$ and $\bar{I}_m$.
$\bar{\gamma}_i$	Phase angle of $\bar{I}_m$ within its operating sector.
θ^-	Initial phase angle of grid voltages (-) sequence.
ω_i	Grid voltage's angular frequency.
ω_0	Input filter's resonant angular frequency.
ω_r	Resonant angular frequency of the resonant controller.

Manuscript received September 26, 2014; revised January 16, 2015; accepted March 26, 2015. Date of publication XXXXXX; date of current version XXXXXX. This work was supported in part by NSERC, Canada Research Chair in Electric Energy Conversion and Power Electronics CRC-EECPE, ETS de Montréal.

Mahmoud Hamouda, is with CRC-EECPE, Ecole de technologie supérieure, Montréal, Québec, Canada, H3C1K3, also affiliated with research unit SAGE, ENISO, University of Sousse, Tunisia (e-mail: *mahmoudhamouda@yahoo.fr*).

Handy Fortin Blanchette is with, CRC-EECPE, Ecole de technologie supérieure, Montréal, Québec, Canada, H3C1K3 (e-mail: *handyblanchette@hotmail.com*).

Kamal Al-Haddad is the head of CRC-EECPE, Ecole de technologie supérieure, Montréal, Québec, Canada, H3C1K3 (e-mail: *Kamal.Al-Haddad@ele.etsmtl.ca*).

Color versions of one or more of the figures in this paper are available online at http://ieeexplore.ieee.org.

Digital Object Identifier XXXXXXX.

This article has been accepted for publication in a future issue of this journal, but has not been fully edited. Content may change prior to final publication. Citation information: DOI 10.1109/TPEL.2015.2421480, IEEE Transactions on Power Electronics

I. INTRODUCTION

Matrix Converters are direct AC/AC power conversion devices that are capable of generating variable frequency and amplitude voltages at their output terminals without using bulky and limited lifetime electrolytic capacitors. This important feature allows for the design of high reliability high power density converters. The Indirect Matrix Converter (IMC) depicted in Fig.1, has two major components namely; the four-quadrant current source rectifier called "grid side converter", and the voltage source inverter referred to as "load side converter". Similar to the direct conventional single stage converter, this topology can achieve near sinusoidal line/load currents, controllable input power factor, regeneration capability, etc. Moreover, it has a more secure and less complex commutation process as well as a simple clamp circuit [1]. Compared to the conventional back to back topology, no additional sensors or regulation loops are required to control the voltage across the dc-link [2] [3] [4]. Over the last years, several research works have showed that matrix converters are suitable for various modern industrial applications such as distributed power generation systems [5] [6], multi-drive systems [7], variable speed drives [8] [9], wind energy [10], unified power flow controller (UPFC) [11], etc.

However, like the conventional grid-tied converters, the expected performances (THD of line currents, THD of output voltages, maximum voltage transfer ratio) of Matrix Converters are considerably decreasing when operating under unbalanced grid voltages. It has been shown in [12] that the input voltage imbalance gives rise to low-order harmonics in the output voltages and input currents waveforms. Therefore, low-frequency ripples are provided in the waveform of the demanded instantaneous active power and the reactive power exchanged with the utility.

On the other hand, the input LC filter of the Matrix Converter introduces an inherent phase shift between the line currents ($i_{a,}i_{b,}i_{c}$) and grid voltages ($E_{a,}E_{b,}E_{c}$) which decreases the input power factor as deeply discussed in references [13] [14] [15] [16] [17]. The resulting reactive power demanded from the power grid will therefore give rise to unwanted power losses in the transmission and distribution lines. When the supply voltages are unbalanced, the power grid becomes more sensitive toward the reactive power demand since the latter includes in addition to the dc component low-frequency ripple components which inherently enlarges the amount of the aforementioned losses. Note that the Matrix Converter has the capability to help in supporting the grid voltages by injecting the appropriate amount of reactive power as has been widely recommended by recent grid codes [18] [19] [20]. In this case, the converter needs to operate with a non-unity input power factor where the line currents are leading their corresponding voltages by a positive phase shift. This operation mode is however not the best suited one since it lowers the maximum voltage transfer ratio and consequently the maximum active power to be transferred to the load. Accordingly, the unity input power factor operation is the most opportune operating mode to be considered when the converter is connected to either balanced or unbalanced grid. Note also that the minimization of the reactive power exchange when the converter is connected to a distorted AC supply has been considered as a key constraint in [21].

Different control methods were proposed in the literature to enhance the performance of Single Stage/ Indirect Matrix Converters operating under unbalanced grid voltages. In [22] [23] [24], several dynamic space vector modulations of the input currents are proposed to enhance their quality and cancel low-order harmonics that are caused by the grid voltages imbalance. However, the impact of these techniques on balancing the load currents was not discussed. In [25], a modulation technique that determines the opportune amplitude and phase angle of the negative sequence of the line currents has been proposed with the aim to improve the quality of the line and load currents respectively. In [26], the authors proposed a modified calculation method of the grid voltages phase angle. This latter was combined with the conventional space vector modulation technique with the aim to enhance the quality of the output voltage waveform. In [27], the authors proposed three modulation methods for the Matrix Converter based on three mathematical constructions of the rectifier and inverter modulation vectors. These methods achieve similar performance in terms of load current quality. As for the line current quality, the third method is a compromise between method I and II in terms of THD and third-order harmonic amplitude. In [28], a feed-forward compensation method of the input voltage imbalance was proposed. It has defined an appropriate unbalanced switching function of the grid side converter so as to cancel the low-order harmonics contents in the voltage across the virtual dc-link. Consequently, balanced output voltages are provided at the load side. In, [29] the authors proposed an active compensation method that uses the clamp capacitor so as to provide balanced output voltages and preserve the maximum value of the voltage transfer ratio.

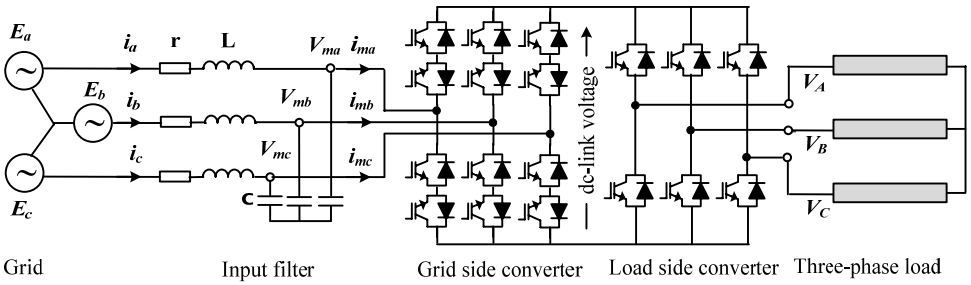

Fig.1 Power circuit of an Indirect Matrix Converter

This article has been accepted for publication in a future issue of this journal, but has not been fully edited. Content may change prior to final publication. Citation information: DOI 10.1109/TPEL.2015.2421480, IEEE Transactions on Power Electronics

A feed-forward compensation method based upon measurement of the instantaneous grid voltages was proposed in [30] with the aim to provide balanced output voltages. In [31] a predictive control algorithm is applied to the converter feeding an induction motor. It has been shown that the proposed strategy presents satisfactory behavior even under unbalanced grid voltages.

On the other hand, the input power factor correction under balanced grid voltages operation has been addressed by many research works [17] [15] [13] [32]. The behavior of the converter has also been investigated under distorted grid voltages [21] [33]. Such a disturbance of the grid voltage is however out of the scope of this work.

This paper proposes an advanced control method of Indirect Matrix Converter operating under unbalanced grid voltages. The proposed controller is designed with the aim to achieve two main goals: 1) the converter should provide balanced output voltages and therefore an almost low-frequency-ripple free active power (constant active power) is demanded from the grid. 2) A near unity input power factor operation should be achieved. The second goal is the main novelty of the paper that has not been addressed by the previous research works.

The manuscript is organized as follows: Section II provides a detailed definition of the instantaneous active and reactive powers under unbalanced grid voltages. The proposed control method of the converter operating under unbalanced grid voltages is explained in sections III and IV respectively. The maximum voltage transfer ratio that can be reached with this method is determined in section V. Finally, several experimental results are presented in section VI and aimed to validate the proposed theoretical approach.

II. Instantaneous Active and Reactive Powers Under Unbalanced Grid Voltages

A three-phase unbalanced grid voltage system without a zero-sequence can be modeled in a stationary reference frame as the sum of positive and negative sequence components [34] [35] , such that:

$$\bar{E} = E^{+}e^{j\omega_i t} + E^{-}e^{j(-\omega_i t-\theta^{-})} \tag{1}$$

E^{+} and $E^{-}$are the peak values of positive and negative sequence components of the grid voltages. θ^{-} is the initial phase angle of the negative sequence, and ω_i is the angular frequency of the grid voltages. In (1) the initial phase angle of the positive sequence is assumed equal to zero.

On the other hand, the quality of input-line currents drawn by Matrix Converters operating under unbalanced grid voltages has been discussed by Casadei et al. in [36] and [12]. In both papers, it has been concluded that the input-line current waveforms depend upon the modulation strategy where two possible methods where evaluated.

- The first modulation method keeps a constant input displacement angle between the instantaneous grid voltage and input current. This method provides non-sinusoidal line currents that include a series of positive-sequence harmonic components of order 2k+1 (k=1, 2,..).
- The second modulation method performs a dynamic modulation of the input displacement angle between the grid voltage vector and input current vector. This method provides sinusoidal but unbalanced line currents where the harmonic spectrum is reduced to one positive and one negative sequence components.

Therefore, according to the second method, sinusoidal and unbalanced line currents can be provided by the Matrix Converter such that:

$$\bar{I} \;= I^{+}e^{j(\omega_i t+\varphi^{+})} + I^{-}e^{j(-\omega_i t-\varphi^{-})} \tag{2}$$

I^{+} and I^{-} are the peak values of the positive and negative sequences of the line currents; φ^{+} and φ^{-} are their initial phase angles. The instantaneous input active power supplied from the grid to the converter is derived by taking the real part of the complex power such that:

$$P^{in} = \frac{3}{2}Real(\bar{E}\,\bar{I}^{*})$$

$$= \frac{3}{2}\begin{Bmatrix} E^{+}I^{+}\cos\varphi^{+} + E^{-}I^{-}\cos(\varphi^{-}-\theta^{-}) \\ +[E^{+}I^{-}\cos\varphi^{-} + E^{-}I^{+}\cos(\varphi^{+}+\theta^{-})]\cos(2\omega_i t) \\ +[-E^{+}I^{-}\sin\varphi^{-} - E^{-}I^{+}\sin(\varphi^{+}+\theta^{-})]\sin(2\omega_i t) \end{Bmatrix}$$

$$= P_0^{in} + P_{c2}^{in}\cos(2\omega_i t) + P_{s2}^{in}\sin(2\omega_i t) \tag{3}$$

Equation (3) shows that the instantaneous active power at the grid connection point consists of a constant term that represents the average value $\left(P_0^{in}\right)$ of the active power as well as cosine and sine terms of twice the grid frequency that are caused by the grid voltage imbalance. Assume the converter's losses are neglected; therefore the ripple terms can be cancelled simply by providing balanced output voltages as will be explained in section IV. On the other hand, it has been adopted in recent literature that the instantaneous reactive power under unbalanced and non-sinusoidal grid voltages can be described in terms of virtual AC voltages that lag the actual grid voltages by 90° [37] as:

$$Q^{in} = E'_a i_a + E'_b i_b + E'_c i_c \tag{4}$$

$E'_{a,b,c}$ are the instantaneous voltages that lag the actual grid voltages by 90°, $i_{a,b,c}$ are the instantaneous line currents. The reactive power is therefore equivalent to the real part of a quadrature complex power and can be defined as follows:

$$Q^{in} = \frac{3}{2}Real(\bar{E}_{\perp}\,\bar{I}^{*})$$

$$= \frac{3}{2}\begin{Bmatrix} -E^{+}I^{+}\sin\varphi^{+} - E^{-}I^{-}\sin(\varphi^{-}-\theta^{-}) \\ +[E^{+}I^{-}\sin\varphi^{-} + E^{-}I^{+}\sin(\varphi^{+}+\theta^{-})]\cos(2\omega_i t) \\ +[E^{+}I^{-}\cos\varphi^{-} + E^{-}I^{+}\cos(\varphi^{+}+\theta^{-})]\sin(2\omega_i t) \end{Bmatrix}$$

$$= Q_0^{in} + Q_{c2}^{in}\cos(2\omega_i t) + Q_{s2}^{in}\sin(2\omega_i t) \tag{5}$$

In a similar manner, one can observe that besides the constant term, a cosine and sine terms of twice the grid frequency appear in the instantaneous input reactive power waveform. In order to achieve a near unity input power factor operation, one should perform an accurate control of the average reactive power as will be explained in the following section.

This article has been accepted for publication in a future issue of this journal, but has not been fully edited. Content may change prior to final publication. Citation information: DOI 10.1109/TPEL.2015.2421480, IEEE Transactions on Power Electronics

III. Input Power Factor Control via the Grid Side Converter

A. Reactive Current Reference Calculation

The input power factor control requires the computation of the opportune line currents phase angles. Indeed, according to the first term of (5), the average reactive power that the converter can exchange with the grid depends on the initial phase angles φ^+ and φ^-. Its reference ($Q^{in}_{0\_ref}$) is therefore defined as:

$$Q^{in}_{0\_ref} = \frac{3}{2}\left[-E^+I^+\sin(\varphi^+_{ref}) - E^-I^-\sin\left(\varphi^-_{ref} - \theta^-\right)\right] \quad (6)$$

Where, φ^+_{ref} and φ^-_{ref} are the initial phase angles references of the positive and negative sequences of the line currents. The expression of φ^+_{ref} is therefore derived as follows:

$$\sin(\varphi^+_{ref}) = -\frac{2}{3}\frac{Q^{in}_{0\_ref}}{E^+I^+} - \frac{E^-I^-}{E^+I^+}\sin\left(\varphi^-_{ref} - \theta^-\right) \quad (7)$$

On the other side, assume that the oscillating components of the input active power (two last terms of (3)) are perfectly compensated as will be discussed in section IV. The conditions that nullify the two ripple terms found in (3) are:

$$\begin{cases} I^- = \dfrac{E^-}{E^+}I^+ & (8.a) \\ \varphi^+_{ref} + \theta^- = \varphi^-_{ref} + \pi & (8.b) \end{cases}$$

According to equations (7) and (8a, 8b), the opportune values of φ^+_{ref} and φ^-_{ref} that allow the converter to exchange $\left(Q^{in}_{0_{ref}}\right)$ with the grid are determined as follows:

$$\begin{cases} \sin(\varphi^+_{ref}) = -\dfrac{2}{3}\dfrac{E^+}{I^+}\dfrac{Q^{in}_{0\_ref}}{(E^+)^2 - (E^-)^2} & (9.a) \\ \varphi^-_{ref} = \varphi^+_{ref} + \theta^- - \pi & (9.b) \end{cases}$$

In order to achieve the control in a dq reference frame synchronized with the positive sequence of grid voltages, one can define the d-q components of grid voltages as well as the line currents such that:

$$\begin{cases} E_d = E^+_d + E^-_d = E^+ + E^-\cos(-2\omega_i t - \theta^-) \\ E_q = E^+_q + E^-_q = 0 + E^-\sin(-2\omega_i t - \theta^-) \end{cases} \quad (10)$$

$$\begin{cases} I_d = I^+_d + I^-_d = I^+\cos\varphi^+ + I^-\cos(-2\omega t - \varphi^-) & (11.a) \\ I_q = I^+_q + I^-_q = I^+\sin\varphi^+ + I^-\sin(-2\omega t - \varphi^-) & (11.b) \end{cases}$$

Substituting (8.a) and (9a, 9b) in (11.b) and rearranging, yields to the opportune references of positive and negative sequences of the line current reactive component as shown in (12.a) and (12.b) hereafter. A detailed mathematical development is given in the appendix.

$$I^+_{q\_ref} = -\frac{2}{3}Q^{in}_{0\_ref}\frac{E^+_d}{(E^+_d)^2 - \left[(E_d - E^+_d)^2 + \left(E_q\right)^2\right]} \quad (12.a)$$

$$I^-_{q\_ref} = \frac{-E^-_q}{E^+_d}I^+_d + \frac{E^-_d}{E^+_d}I^+_{q\_ref} \quad (12.b)$$

One can verify from (11.b) and (12a, 12b) that the q component of the positive sequence consists of a constant term $\left(I^+_{q\_ref}\right)$ that depends only on the average reactive power reference. The negative sequence component $\left(I^-_{q\_ref}\right)$ consists of a ripple term oscillating at twice the grid frequency. This ripple term depends on the dq components of positive and negative sequences of the grid voltages, as well as the dq components of the positive sequence of the line currents. These computed references are subsequently used as input references to the PIR control loop that is presented hereafter.

B. PIR Based Closed-loop Controller

With the aim to design the appropriate controller which allows an accurate tracking of the opportune current references computed by (12.a) and (12.b), we should first determine the dynamics of the line current reactive component i_q. Using Kirchhoff laws, the reactive components of the line current and capacitor voltage can be expressed in a synchronous reference frame [17] [38]:

$$\frac{d}{dt}i_q = -\frac{r}{L}i_q - \omega_i\, i_d + \frac{1}{L}E_q - \frac{1}{L}V_{mq} \quad (13.a)$$

$$\frac{d}{dt}V_{mq} = -\omega_i V_{md} + \frac{1}{c}i_q - \frac{1}{c}i_{mq} \quad (13.b)$$

As can be seen, the input current i_{mq} that is considered as the control-law does not appear explicitly in the first derivative of i_q. By differentiating (13.a) and using (13.b), we can obtain the dynamics of i_q arranged in a canonical controllable form as shown in (13.c) where $\omega_0 = \frac{1}{\sqrt{Lc}}$ is the input filter resonant angular frequency.

$$\begin{aligned} \frac{d^2}{dt^2}i_q = & -\frac{r}{L}\frac{d}{dt}i_q - \omega_0^2\, i_q + \omega_0^2\, i_{mq} \\ & - \omega_i\frac{d}{dt}i_d + \frac{1}{L}\frac{d}{dt}E_q + \frac{\omega_i}{L}V_{md} \end{aligned} \quad (13.c)$$

Reporting (13.c) in Laplace domain, yields the transfer function described by (13.d) where $Q_f = \frac{1}{r\sqrt{\frac{c}{L}}}$ is the input filter quality factor.

$$i_q\left(\frac{s^2}{\omega_0^2} + \frac{1}{Q_f\,\omega_0}s + 1\right) = \underbrace{i_{mq}}_{control-law} - \underbrace{\left(\frac{\omega_i}{\omega_0^2}\right)s\, i_d}_{coupling\ term} + \underbrace{\left(\frac{1}{L\omega_0^2}\right)s\, E_q + \left(\frac{\omega_i}{L\omega_0^2}\right)V_{md}}_{disturbance\ terms} \quad (13.d)$$

The transfer function (13.d) shows that in addition to the control-law i_{mq}, there exist one coupling and two disturbance terms that should be compensated by the regulator. The use of a PI regulator with an appropriate compensation of the additional terms found in (13.d) can perform a zero steady-state tracking error of the current reference only if the latter is

This article has been accepted for publication in a future issue of this journal, but has not been fully edited. Content may change prior to final publication. Citation information: DOI 10.1109/TPEL.2015.2421480, IEEE Transactions on Power Electronics

a dc signal. Indeed, the key limitation of PI controllers is their inability to perform a perfect tracking of ac reference signals [39]. Accordingly, the ripple term existing in the current reference leads to amplitude and phase tracking errors if only a conventional PI regulator is used. Therefore, the PI controller is reinforced with a resonant term with a resonant frequency of twice the grid frequency. The transfer function of an ideal resonant controller is shown in equation (14), where K_{IR} and $\omega_r = 2\omega_i$ are the gain and resonant angular frequency of the controller.

$$H_R(s) = K_{IR}\frac{s}{s^2+\omega_r^2} \tag{14}$$

In open-loop, $H_R(s)$ provides an infinite gain at twice the grid frequency which ensures an accurate tracking (in closed-loop) of the double-frequency ripple component of the reference current, as well as disturbance rejection for signals pulsating at the resonant frequency. These benefits are achieved without affecting the high frequency stability [40] [41] [42]. However, the infinite gain and narrow bandwidth of the resonant controller may cause instability due to grid frequency deviation and discretization errors [43]. Hence, in order to avoid stability problems, a damped resonant term (15.a) is used instead of (14).

$$H_{R\_damp}(s) = K_{IR}\frac{K_{damp}\ \frac{\omega_r}{Q_{damp}}s}{s^2+\frac{\omega_r}{Q_{damp}}s+\omega_r^2} \tag{15.a}$$

K_{damp} and Q_{damp} are the damped gain and quality factor respectively. The transfer function defined in (15.a) provides a complete separation of the gain and bandwidth at resonant frequency such that:

$$\begin{cases} H_{R_{damp}}(\omega=\omega_r) = K_{IR}K_{damp} \\ BW(\omega=\omega_r) = \dfrac{\omega_r}{Q_{damp}} \end{cases} \tag{15.b}$$

Moreover, one can observe that the standard ideal controller of (14) is a particular case of (15.a) with $Q_{damp} \gg \omega_r$ and $K_{damp} = \frac{Q_{damp}}{\omega_r}$ Accordingly, the opportune control-law i_{mq} is determined by multiplying the error signal by the *PIR* controller transfer function and removing the coupling and disturbance terms of (13.d) which yields:

$$i_{mq} = \underbrace{\left[K_p + \frac{K_I}{s} + K_{IR}\frac{K_{damp}\ \frac{\omega_r}{Q_{damp}}s}{s^2+\frac{\omega_r}{Q_{damp}}s+\omega_r^2}\right]}_{PIR\ controller}\underbrace{\left[I_{q\_ref}^{+} + I_{q\_ref}^{-} - i_q\right]}_{error\ signal} + \underbrace{\left(\frac{\omega_i}{\omega_0^2}\right)s\ i_d}_{coupling\ compensation} - \underbrace{\left(\frac{1}{L\omega_0^2}\right)s\ E_q - \left(\frac{\omega_i}{L\omega_0^2}\right)V_{md}}_{disturbance\ rejection} \tag{16.a}$$

As can be seen, equation (16.a) requires the calculation of the first derivative of i_d and $E_q$which reduces the accuracy of the control-law for real-time implementation. An equivalent expression to the first derivative of E_q can be deduced from (10) as follows:

$$\frac{d}{dt}E_q = -2\omega_i\ E_d^{-} \tag{16.b}$$

On the other hand, the term $(s\ i_{sd})$ can be substituted by the mathematical equation that describes the dynamics of i_d in the dq frame such that:

$$\frac{d}{dt}i_d = -\frac{r}{L}i_{sd} + \omega_i\ i_q + \frac{1}{L}E_d - \frac{1}{L}V_{md} \tag{16.c}$$

Plugging equations (16.b) and (16.c) into (16.a), an equivalent expression of the control-law which is more suitable for real-time implementation is therefore obtained:

$$i_{mq} = \underbrace{\left[K_p + \frac{K_I}{s} + K_{IR}\frac{K_{damp}\ \frac{\omega_r}{Q_{damp}}s}{s^2+\frac{\omega_r}{Q_{damp}}s+\omega_r^2}\right]}_{PIR\ controller}\left[I_{q\_ref}^{+} + I_{q\_ref}^{-} - i_q\right] + \frac{1}{\omega_0^2}\left[-\omega_i\frac{r}{L}i_d + \omega_i^2 i_q + \frac{\omega_i}{L}E_d - \frac{2\omega_i}{L}V_{md} + \frac{2\omega_i}{L}\ E_d^{-}\right] \tag{16.d}$$

The control-law i_{mq} is thereafter used to determine the opportune direction of the input current space vector such that:

$$\varphi_i = tan^{-1}\left(\frac{i_{mq}}{i_{md}}\right) \tag{17}$$

Where φ_i is the instantaneous phase angle between the positive sequence of the grid voltage space vector ($\bar{E}^{+} = E^{+}e^{j\omega t}$) and the converter input current space vector namely $\bar{I}_m$ as illustrated in Fig.2. Since i_{md} is the direct component of modulated currents ($i_{ma,mb,mc}$), therefore, it cannot be sensed with the aim to compute the instantaneous value of (17). By neglecting the power losses in the high frequency filter, one can assume the direct component i_d is similar to i_{md}. Consequently, it can be used in equation (17) without loss of accuracy. Finally, the input current's direction, that is determined according to (17), can be synthesized using the SVPWM technique which consists in impressing at each sampling period the two active vectors adjacent to $\bar{I}_m$ with the opportune duty cycles, namely d_{1R} and d_{2R} as depicted in Fig.2.

C. *Stability Analysis*

The steady state and dynamic performance of the controller greatly depend on the gain of proportional, integral, and resonant terms.

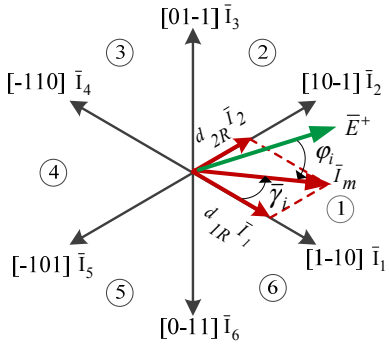

Fig.2 Synthesis of $\bar{I}_m$ vector using SVPWM method

This article has been accepted for publication in a future issue of this journal, but has not been fully edited. Content may change prior to final publication. Citation information: DOI 10.1109/TPEL.2015.2421480, IEEE Transactions on Power Electronics

Basically, the high frequency system response (transient response) is managed by the proportional gain whereas; the steady-state error and the phase margin are determined by the integral and resonant gains. The most commonly used approach to obtain the appropriate gains and to study the system's stability is usually based on Bode diagrams and the phase margin criterion that require precise knowledge of the open-loop transfer function of the plant under control. Substituting firstly (16.a) into (13.d), a closed-loop relationship between i_q and its reference $I_{q\_ref} = I^{+}_{q\_ref} + I^{-}_{q\_ref}$ is thereby derived as follows:

$$i_q\left(\frac{s^2}{\omega_0^2}+\frac{1}{Q_f\,\omega_0}s+1\right)= \underbrace{\left[K_p+\frac{K_I}{s}+K_{IR}\frac{K_{damp}\ \frac{\omega_r}{Q_{damp}}s}{s^2+\frac{\omega_r}{Q_{damp}}s+\omega_r^2}\right]}_{PIR\ controller}\underbrace{\left[I^{+}_{q\_ref}+I^{-}_{q\_ref}-i_q\right]}_{error\ signal} \quad (18)$$

It is now straightforward to describe the closed-loop control system computed in (18) by the block diagram of Fig.3 hereafter which illustrates clearly the open-loop forward path. Consequently, the ideal open-loop transfer function namely G(s) can be expressed as follows:

$$G(s)=\left[K_p+\frac{K_I}{s}+K_{IR}\frac{K_{damp}\ \frac{\omega_r}{Q_{damp}}s}{s^2+\frac{\omega_r}{Q_{damp}}s+\omega_r^2}\right]\frac{1}{\left(\frac{s^2}{\omega_0^2}+\frac{1}{Q_f\,\omega_0}s+1\right)} \quad (19)$$

Fig.4a displays the magnitude and phase Bode diagrams of G(s) obtained with $K_p = 0.05$ and two different values of the integral and resonant gains ($K_I = K_{IR} = 15\ and\ 20$). The loop gain curve shows 5 different cross-over frequencies for each case. The first one (f_{c1}) is due to the integral term of the controller and is located at the neighboring of dc frequencies. Two others cross-over frequencies (f_{c2}, f_{c3}) are located around the controller's resonant frequency. The remaining two cross-over frequencies (f_{c4}, f_{c5}) are located around the input filter resonant frequency (≈1kHz). The most critical case is located at the right side of the input filter resonant frequency since the corresponding phase margin is the closest to -180° phase line. On the other hand, it can be observed clearly that a larger value of the resonant term increases the gain at the resonance frequency of the controller implying that a better accuracy is achieved in steady-state operation. However, this benefit is obtained at the cost of phase margin decrease as the resonant gain increases.

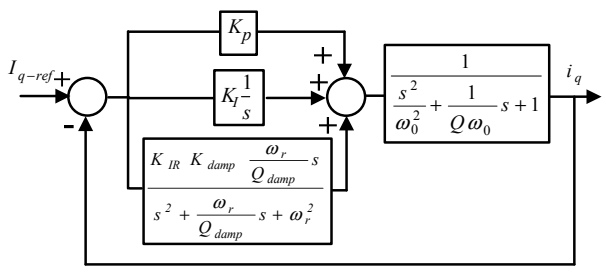

Fig.3 Schematic Block diagram of the closed-loop control system described by (18)

Fig.4a shows also that the phase margins obtained with both values of K_{IR} are too small to ensure a robust stability. A further decrease of K_{IR} is not suitable since it will worsen the accuracy at steady-state operation. The only permissible solution is therefore to decrease the proportional gain K_p. Fig.4b displays the Bode diagrams obtained with $K_I = K_{IR} = 15$ and $K_p = 0.03$. The obtained phase margin is theoretically greater than 40°. However, it is worthy to point out that the above analysis was done without considering the effect of the delays caused by the sampling phenomenon as well as by the current and voltage transducers. Equation (20) gives a more realistic open-loop transfer function including one sampling period delay(e^{-Ts}).

$$G(s)= e^{-Ts}\left[K_p+\frac{K_I}{s}+K_{IR}\frac{K_{damp}\ \frac{\omega_r}{Q_{damp}}s}{s^2+\frac{\omega_r}{Q_{damp}}s+\omega_r^2}\right]\frac{1}{\left(\frac{s^2}{\omega_0^2}+\frac{1}{Q_f\,\omega_0}s+1\right)} \quad (20)$$

The corresponding Bode plot of Fig.4c (black curve) shows clearly that the phase margin becomes smaller and thereby is not sufficient to ensure a robust stability. It is therefore obvious to conclude that a lower value of K_p that provides a gain below the 0 dB line is mandatory to avoid the stability problem at the resonant frequency of the filter. Fig.4c (gray curve), shows the Bode plot for $K_p = 0.01$; as compared to the previous case (black curve), it is clear that the filter gain at resonance frequency is well damped so that the gain curve will never cross over the 0 dB line at this critical frequency. Moreover, the gains at the dc and the controller's resonant frequencies remain unchanged implying that no negative impact will occur on the steady state error. It was experimentally tested that a suitable value of the proportional gain below 0.03 is $K_p = 0.01$. This value leads to a satisfactory performance for line current THD which is an important constraint.

D. Extension to Four-Wire Configuration

As compared to the three-wire converters structures, the four-wire configuration introduces a zero-sequence current path which is helpful to achieve a better power control performance [20]. Therefore, to extend the proposed control-theory to the four-wire configuration, it is mandatory to design an additional loop so as to enable the controllability of the zero-sequence current flowing through the neutral point.

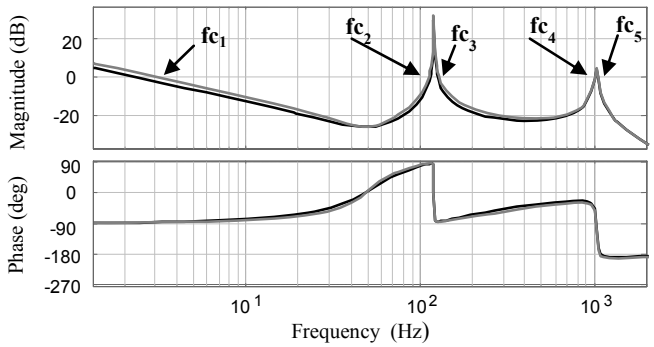

Fig.4a Bode plot of the open-loop transfer function G(s) obtained with K_p= 0.05 and two values of K_I and K_{IR} (black curve: $K_I = K_{IR} = 15$; gray curve: $K_I = K_{IR} = 20$)

This article has been accepted for publication in a future issue of this journal, but has not been fully edited. Content may change prior to final publication. Citation information: DOI 10.1109/TPEL.2015.2421480, IEEE Transactions on Power Electronics

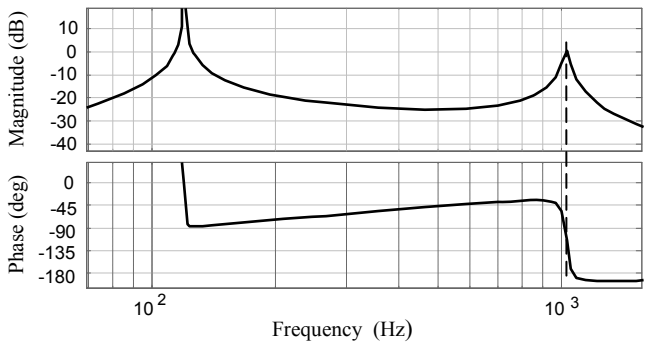

Fig.4b Bode plot of the open-loop transfer function G(s) obtained with K_p = 0.03 and $K_I = K_{IR}$ = 15

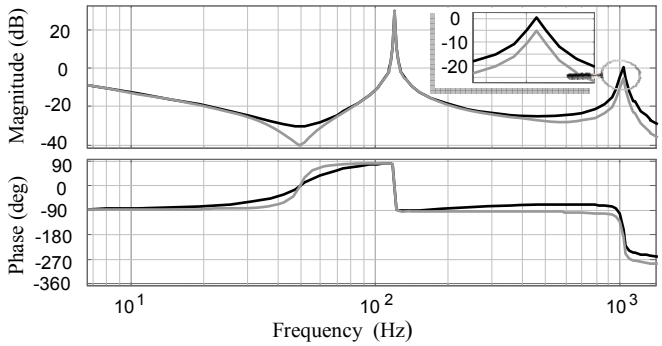

Fig.4c Bode plot of the open-loop transfer function including a delay of one sampling period; black curve K_p = 0.03 and $K_I = K_{IR}$ = 15; gray curve K_p = 0.01 and $K_I = K_{IR}$ = 15

The authors underline that, to their best knowledge, the most commonly used Matrix Converters topologies are connected to grid through a three-wire system. The four-wire system has been adopted in case of unbalanced load which is out the scope of this paper. In this case, the common neutral point of the load was connected to the midpoint of an additional leg of the inverter stage giving rise to a modified topology named the Four-Leg Indirect Matrix Converter [44].

IV. Control of Output Voltages and Active Power

For the sake of simplicity, the converter's losses are assumed to be neglected. Therefore, if balanced output voltages and currents are provided at the load side of the converter, the input active power is inherently free of double-frequency ripple components. For this purpose, a straightforward method will be presented hereafter so as to provide balanced output voltages when the converter is tied to an unbalanced grid. Therefore, a real-time estimator of the dc-link voltage is developed based upon the measurement of instantaneous grid voltages as well as an average switching function of the grid side converter.

As an example, assume the input current reference vector $\bar{I}_m$ is residing within sector 1 of the complex plane as illustrated in Fig.2. In this situation, the upper switch of phase-leg *a* is turned on over the full switching period while the lower switches of phase-legs *b* and *c* are modulated with duty cycles d_{1R} and d_{2R} respectively. The remaining power devices are switched off. An *average switching function* $\langle \bar{S}_G \rangle_{Tc}$ of the grid side converter can thereafter be defined within a switching period (T_c) as given in equation (21.a) where, $a = e^{j\frac{2\pi}{3}}$:

$$\langle \bar{S}_G \rangle_{Tc} = \frac{2}{3}(1 - a\, d_{1R} - a^2\, d_{2R}) \qquad (21.\text{a})$$

Equation (21.a) in turn can be generalized for the six possible positions of the input current space vector $\bar{I}_m$ in the complex plane as shown in equation (21.b), where $d_{a,b,c}$ are duty cycles assigned to phase-legs *a*, *b*, and *c*.

$$\langle \bar{S}_G \rangle_{T_c} = \frac{2}{3}(d_a + a\, d_b + a^2\, d_c) \qquad (21.\text{b})$$

On the other hand, let $\bar{\gamma}_i$ be defined as the instantaneous phase angle of $\bar{I}_m$ within its operating sector as seen in Fig 2.

$$\bar{\gamma}_i = \omega_i t - (K_i - 1)\frac{\pi}{3} + \frac{\pi}{6} + \varphi_i \qquad (22.\text{a})$$

In (22.a) K_i is the sector number where $\bar{I}_m$ is lying. In this case, the duty cycles d_{1R} and d_{2R} can be expressed as a function of $\bar{\gamma}_i$ such that [4]:

$$d_{1R} = \frac{\sin\left(\frac{\pi}{3} - \bar{\gamma}_i\right)}{\cos\left(\frac{\pi}{6} - \bar{\gamma}_i\right)}; \quad d_{2R} = \frac{\sin(\bar{\gamma}_i)}{\cos\left(\frac{\pi}{6} - \bar{\gamma}_i\right)} \qquad (22.\text{b})$$

Therefore, equation (21.b) can be rewritten as follows:

$$\langle \bar{S}_G \rangle_{T_c} = \frac{1}{\cos\left[\omega_i t - (K_i - 1)\frac{\pi}{3} + \varphi_i\right]} e^{j(\omega_i t + \varphi_i)} \qquad (23)$$

It follows that the average value of the dc-link voltage can be expressed as:

$$\begin{aligned} \langle V_{dc} \rangle_{T_c} &= \frac{3}{2} Real\ \left[\langle \bar{S}_G \rangle_{T_c} \bar{E}^*\right] \\ &= \frac{3}{2} \frac{E^+ cos\varphi_i + E^- \cos(2\omega_i t + \theta^- + \varphi_i)}{\cos\left[\omega_i t - (K_i - 1)\frac{\pi}{3} + \varphi_i\right]} \end{aligned} \qquad (24)$$

$\bar{E}^*$ is the conjugate space vector of the grid voltages. φ_i is the instantaneous phase angle between the positive sequence of the grid voltage space vector and $\bar{I}_m$ that is computed in real time by the PIR controller as explained above in section III/B. Consequently, the real-time estimator should operate downstream of the PIR based control loop. On the other hand, one can observe that the nominator of the estimated dc-link voltage (equation (24)) includes a double-frequency ripple term due to the grid imbalance. Such term that appears in the denominator is due to modulation scheme of the grid side converter. Note also that the upper term of (24) needs less computational burden as compared to the lower term of the same equation, since it avoids using trigonometric functions and the division operator. Therefore, the real-time implementation of the dc-link voltage estimator is based on the upper term of (24) where the value of $\langle \bar{S}_G \rangle_{T_c}$ is updated according to (21.b).

Assume now the dc-link voltage is constant within a sampling period and is equal to its average value. A balanced output voltage system can therefore be provided at the load side simply by impressing the active vectors of the load side

This article has been accepted for publication in a future issue of this journal, but has not been fully edited. Content may change prior to final publication. Citation information: DOI 10.1109/TPEL.2015.2421480, IEEE Transactions on Power Electronics

converter by an unbalanced system of duty cycles as shown in (25) where d_{1I} and d_{2I} stand for the applied duty cycles of the two active vectors adjacent to the reference space vector $\bar{V}_{o\_ref}$. The latter is equivalent to the balanced output voltages V_A, V_B, and V_C. $\hat{V}_o$ and $\bar{\theta}_o$ are the amplitude and instantaneous phase angle within its operating sector of the reference space vector $\bar{V}_{o\_ref}$ as depicted in Fig.5.

$$d_{1I} = \sqrt{3}\frac{\hat{V}_o}{\langle V_{dc}\rangle_{T_c}}\sin\left(\frac{\pi}{3}-\bar{\theta}_o\right);\ d_{2I} = \sqrt{3}\frac{\hat{V}_o}{\langle V_{dc}\rangle_{T_c}}\sin(\bar{\theta}_o) \quad (25)$$

Fig.6 shows a general block diagram of the proposed controller. A multiple reference frame PLL (MRF-PLL) is implemented so as to achieve a perfect synchronization with the positive sequence of the grid voltages as well as a minimized ripple in the estimated phase angle waveform. The implementation of reactive current references $I^+_{q\_ref}$ and $I^-_{q\_ref}$ according to (12.a-b) requires the real-time computation of signals E_d^+, E_q^+, E_d^-, E_q^-, and I_d^+. E_d^+, E_q^+, E_d^-, and E_q^- are directly extracted from the MRF-PLL block while a low-pass filter is used to extract I_d^+ from the signal i_d . Once the current references are determined, the control-law i_{mq} and the instantaneous phase angle φ_i are computed according to (16.d) and (17). This allows performing the SVPWM scheme of the grid side converter and also the estimation of the dc-link voltage according to the upper term of (24) and (21.b). Therefore the SVPWM of the load side converter is performed according to (25). Finally, the block "switching pattern distribution" generates the appropriate gating pulses for the grid side and load side parts of the Indirect Matrix Converter.

V. Maximum Voltage Transfer Ratio

Assume firstly that the load side converter operates as a conventional voltage source inverter supplied by a constant dc source. The relationship between the amplitude of the output voltage fundamental component and the dc source voltage is defined as a function of the inverter modulation index M_I such that:

$$\hat{V}_o = M_I\frac{V_{dc}}{2} \quad (26)$$

It is well known that when the output voltages are modulated with the SVPWM scheme, the maximum value of M_I is $M_{Imax} = 1.155$. On the other hand, Fig.7 displays the grid voltage vector locus where $\bar{E}^+ = E^+e^{j\omega_i t}$ is the vector equivalent to the positive sequence component and rotating counterclockwise; $\bar{E}^- = E^-e^{j(-\omega_i t-\theta^-)}$ is the vector equivalent to the negative sequence component and rotating clockwise.

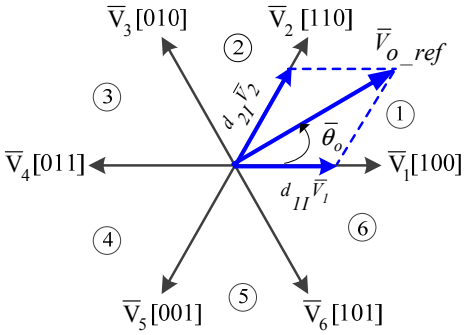

Fig.5 Synthesis of $\bar{V}_{o\_ref}$ vector using SVPWM method

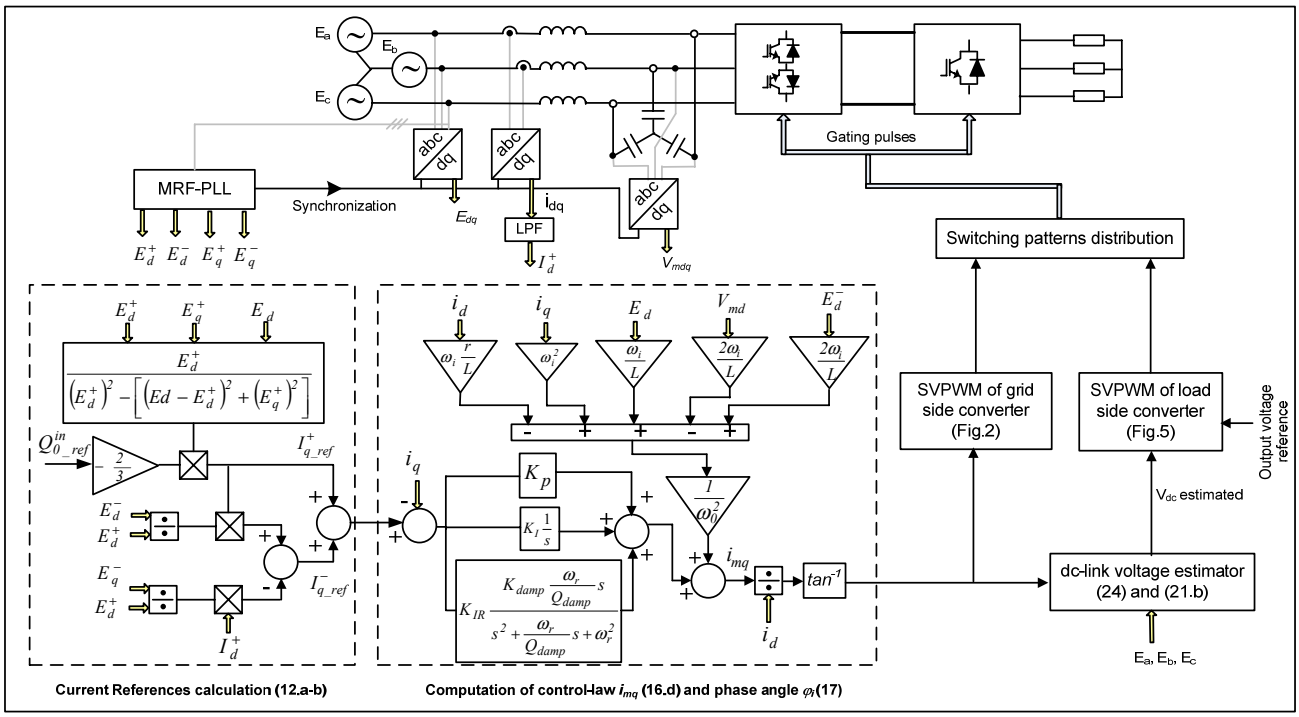

Fig.6 Simplified schematic diagram of the control-law

This article has been accepted for publication in a future issue of this journal, but has not been fully edited. Content may change prior to final publication. Citation information: DOI 10.1109/TPEL.2015.2421480, IEEE Transactions on Power Electronics

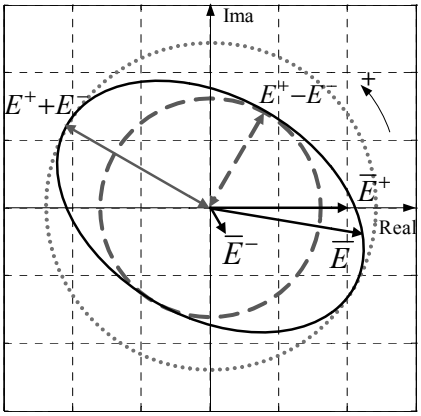

Fig.7 Root locus of the grid voltage vector $\bar{E}$ rotating in an elliptical trajectory

Fig.7 shows clearly that the grid voltage vector $\bar{E}$ is rotating in an elliptical trajectory because of the negative sequence component. Therefore, the amplitude of $\bar{E}$ is time varying while being bounded between the amplitudes of the major and minor axis. Its minimum value is equal to $(E^+ - E^-)$ and occurs when $\bar{E}^+$and $\bar{E}^-$ have the same direction but opposite sense i.e.

$$\omega_i t = -\omega_i t - \theta^- + k\pi \ (k = 1,3, \dots) \tag{27}$$

The maximum amplitude of $\bar{E}$ is equal to $(E^+ + E^-)$ and occurs when $\bar{E}^+$and $\bar{E}^-$ are oriented toward the same direction and sense i.e.

$$\omega_i t = -\omega_i t - \theta^- + 2k\pi \ (k = 1,3, \dots) \tag{28}$$

Therefore, to determine the maximum voltage transfer ratio, it is obvious to consider the worst case corresponding to the minimum amplitude of the grid voltage vector. Substituting (27) in (24) the expression of V_{dc} corresponding to this worst case scenario is therefore given by:

$$\langle V_{dc} \rangle_{T_c} = \frac{3}{2} \frac{(E^+ - E^-) cos\varphi_i}{\cos\left[\omega_i t - (K_i - 1)\frac{\pi}{3} + \varphi_i\right]} \tag{29}$$

The ripple term in the denominator of (29) is obviously due to the modulation phenomenon of the grid side converter. Therefore the lowest amplitude of $\langle V_{dc} \rangle_{T_c}$ is achieved when the denominator is equal to 1 which yields to:

$$\langle V_{dc} \rangle_{T_{c\_min}} = \frac{3}{2}(E^+ - E^-) cos\varphi_i \tag{30}$$

It is now evident to conclude that the maximum amplitude of the output voltage fundamental component in the linear region operation can be found by combining equations (30), (26) and substituting M_I by its maximum value (M_{Imax}) which yields:

$$\hat{V}_{omax} = M_{Imax} \frac{3}{4}(E^+ - E^-) cos\varphi_i \tag{31}$$

The maximum voltage transfer ratio defined as $q_{max} = \hat{V}_{omax}/E^+$ is thereby deduced from (31) as shown in (32) where $u = E^-/E^+$ is the grid voltage imbalance degree.

$$\begin{aligned} q_{max} &= \frac{\hat{V}_{omax}}{E^+} = M_{Imax} \frac{3}{4}(1-u) cos\varphi_i \\ &= 0.866 \ (1-u) cos\varphi_i \end{aligned} \tag{32}$$

If $u = 0$, case of balanced system, one can find the usual q_{max} value : $q_{max} = 0.866 \ cos\varphi_i$

VI. Experimental Validation

A laboratory prototype of an Indirect Matrix Converter connected to unbalanced three-phase voltage sources and feeding a three-phase star-connected RL-load is built to evaluate the performance of the proposed control methodology. A photo of the realized prototype is illustrated in Fig.8. The voltage imbalance is provided using three single-phase autotransformers. Both control and modulation algorithms were fully implemented on the DSP processor TMS 320F28335 of TI with a switching frequency and a sampling rate of 7.5 kHz. The parameters of the experimental setup and controller used in the following tests are detailed in table I. The average reactive power reference is set to zero $(Q^{in}_{0_{ref}} = 0)$.

The performance of the proposed control method is first evaluated under a 15% decrease of one phase amplitude as illustrated in Fig.9a. The distortions observed in the grid voltages waveforms are caused by nonlinear loads connected to the grid. The target output to the input voltage transfer ratio with respect to the positive-sequence amplitude is set to q = 0.75 while the load frequency is set to f_o = 70 Hz. Fig.9b shows the waveforms of the input filter capacitors voltages. One can observe, in addition to the same voltage imbalance dictated by the grid, high frequency distortion mainly due to the high switching frequency current harmonics flowing into the capacitors.

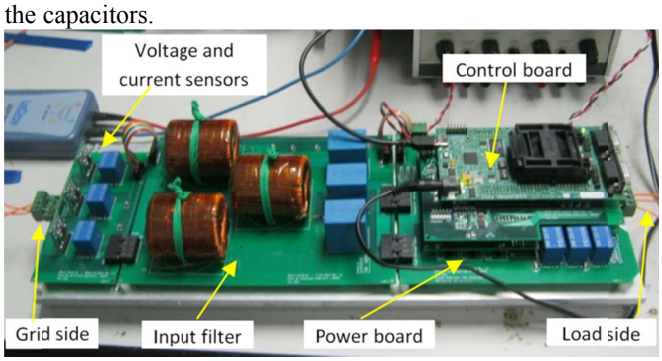

Fig.8 Photo of the IMC laboratory prototype

Table I: System parameters used for the experimental setup

Parameter name	Value
Input filter capacitance (c)	12 µF
Input filter inductance (L)	2 mH
Load inductance (L_L)	9.5 mH
Load resistance (R_L)	12.5 Ω
Proportional gain of PI term (K_p)	0.01
Integral gain of PI term (K_I)	15
Gain of resonant term (K_{IR})	15
Damping gain of resonant term (K_{damp})	2
Quality factor of the resonant term (Q_{damp})	300

This article has been accepted for publication in a future issue of this journal, but has not been fully edited. Content may change prior to final publication. Citation information: DOI 10.1109/TPEL.2015.2421480, IEEE Transactions on Power Electronics

Figs.10a-b illustrate a phase to neutral output voltage waveform as well as the three load currents. Despite the grid voltage imbalance, the converter is able to provide three-phase balanced and sinusoidal load currents as observed in Fig.10b. The immediate consequence of balancing the load currents/voltages can be observed in the active power waveform shown in Fig.11. The latter is effectively free of double-frequency ripple mainly caused by the grid voltage imbalance. Moreover, except the high-frequency ripple, the obtained active power waveform is almost constant in steady state operation. This result emphasizes the effectiveness of the load side converter's control methodology as well as the accuracy of the proposed estimator.

On the other hand, Fig.12a shows that the currents injected into the grid (i_a, i_b, and i_c) are effectively sinusoidal and unbalanced. The amplitudes of their fundamental components are 3.15A (i_a), 2.87A (i_b) and 2.94A (i_c) respectively. The THD measured using the power analysis tool found on the scope "Teldyne Lecroy" HDO6104-HD4096 is 6.12% for i_a, 6.4% for i_b, and 6.34% for i_c respectively. Moreover, by inspecting Fig.12b, one can observe that the line currents are almost in phase with their corresponding grid voltages i.e. a near unity input power factor is achieved. This interpretation is emphasized by the result of Fig.11 which shows clearly that the average reactive power is very close to zero.

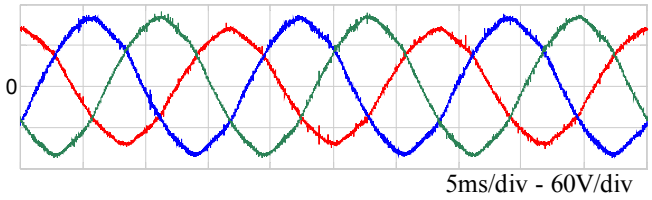

Fig.9a Unbalanced line to neutral grid voltages. The imbalance is obtained by decreasing of 15% one phase amplitude.

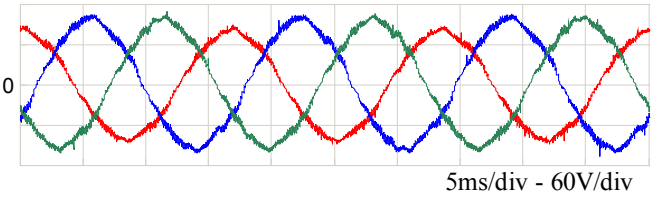

Fig.9b Voltages across the input filter capacitors (V_{ma}, V_{mb}, and V_{mc})

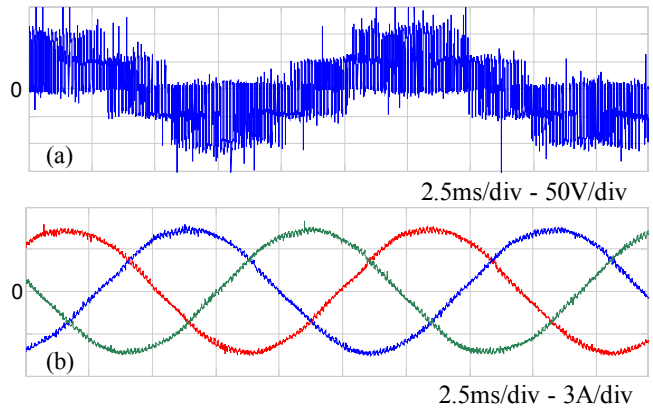

Fig.10 Load side waveforms; (a) phase to neutral output voltage – (b) load currents i_A, i_B, and i_C

Thus, it can be concluded that the proposed reactive power loop performs a satisfactory steady-state tracking of the reference $Q_{0\_ref}^{in}$ which was set to zero. It is also clear that the reactive power waveform includes a ripple component oscillating at twice the grid frequency. This result is quite normal as expected by equation (5) of the theoretical analysis carried out in section II. Note also that only the low-frequency ripple of the active power is removed. Indeed, in the existing control theories applied to converters tied to unbalanced grid voltages, when the constraint of sinusoidal line currents is imposed, therefore, it is not possible to compensate perfectly and simultaneously active and reactive power ripples in case of three-phase three-wire conversion topologies [45].

As in practice, the Indirect Matrix Converter should operate with different output voltages and frequencies; the performance of the proposed methodology is therefore tested for an abrupt change of both q (q changed from 0.75 to 0.55) and f_o (f_o changed from 70 to 50 Hz). Fig.13 shows that the system performs very well during both steady-state and transient operation. Moreover, for the two operating points the line current remains in phase with its corresponding grid voltage.

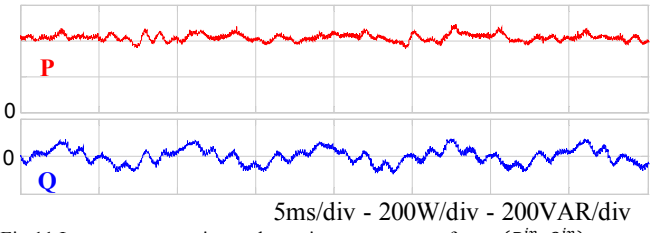

Fig.11 Instantaneous active and reactive powers waveforms (P^{in}, Q^{in})

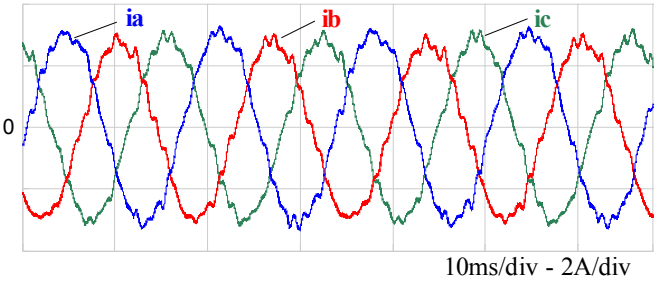

Fig.12a Line currents i_a, i_b, and i_c

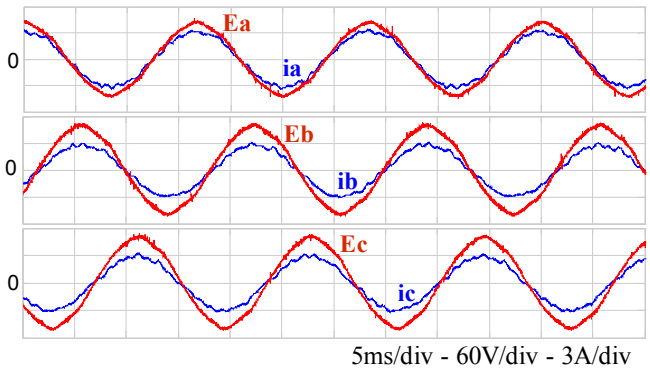

Fig.12b Line to neutral grid voltages and line currents (E_a,i_a), (E_b,i_b), and (E_c, i_c)

This article has been accepted for publication in a future issue of this journal, but has not been fully edited. Content may change prior to final publication. Citation information: DOI 10.1109/TPEL.2015.2421480, IEEE Transactions on Power Electronics

In Fig.14 are shown the active and reactive power waveforms. It can be observed that the average value of the reactive power is not affected by the abrupt decrease of the active power and remains very close to zero i.e. the converter remains operating at near unity input power factor.

Since no closed-loop control algorithms were proposed in the earlier literature so as to control the input power factor of IMC operating under unbalanced grid voltages, a comparative study with earlier methods has no meaning. However, in order to show the benefits of the proposed method, the same previous test was carried out without the reactive power loop (the PIR controller and disturbance rejection terms are disabled). Fig.15 shows clearly that the average reactive power is different from zero for the two operating points.

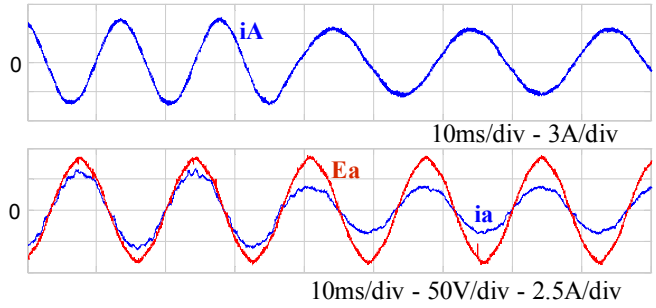

Fig.13 Load current (i_A), line to neutral grid voltage Ea, and line current (i_a) during an abrupt decrease of q and f_o.

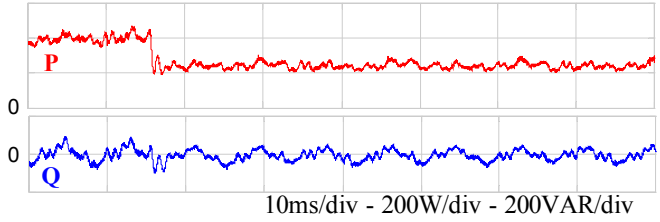

Fig.14 Instantaneous active and reactive powers P^{in}, Q^{in} during an abrupt decrease of the voltage transfer ratio q and f_o .

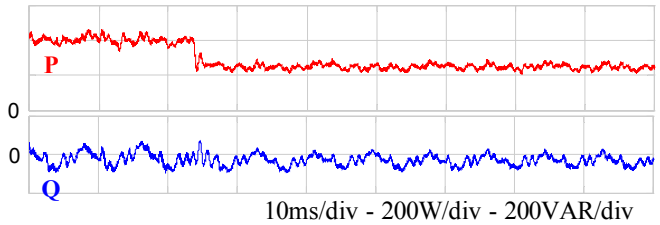

Fig.15 Instantaneous active and reactive powers P^{in}, Q^{in} during an abrupt decrease of q and f_o (with no reactive power control loop).

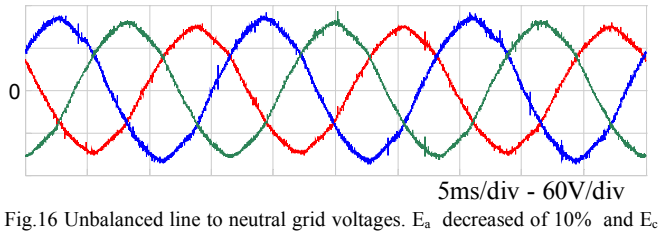

Fig.16 Unbalanced line to neutral grid voltages. E_a decreased of 10% and E_c decreased of 5% .

Obviously, a further decrease of q will lead to a more important variation of the reactive power exchanged with the grid. Therefore, in the absence of the reactive power control loop, when the converter is forced to operate at low value of q, the input power factor may reach lower value, which will definitely have negative impact on the grid.

In a second test, the amplitude of E_a is decreased by 10% while the one of E_c is decreased by 5% as shown in Fig.16. The result illustrated in Fig.17 shows clearly that converter is also able to provide balanced current to the load. Moreover, the line currents remain sinusoidal and in phase with their corresponding grid voltages as shown in Fig.18. Therefore, the unity input power factor operation is also achieved. These results confirm that the proposed reactive power controller and dc-link voltage estimator operate perfectly even under these unfavorable conditions of the grid voltages.

VII. Conclusion

This paper introduced an advanced control method for an Indirect Matrix Converter operating under unbalanced grid voltages in order to provide balanced output voltages and achieve a near unity input power factor operation. The benefit of the proposed reactive power controller is the use of a single control loop thanks to the feature of the PIR controller which is able to perform the tracking of both dc and oscillating terms existing in the input current reference. The experimental tests showed that this controller operates very efficiently and confirm its capability to drive the converter with a near unity input power factor even under variable active power demanded by the load. On the other hand, a real-time estimator of the dc-link voltage was successfully constructed based on the instantaneous measurement of grid voltages as well as an average switching function of the grid side converter.

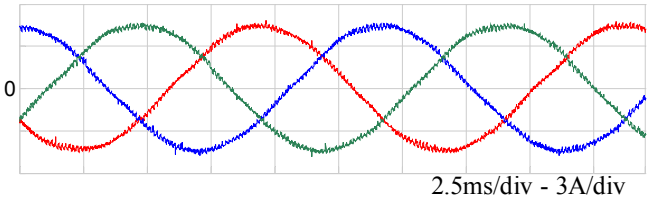

Fig.17 Steady state load currents i_A, i_B, and i_C obtained under 10% decrease of E_a and 5% of E_c .

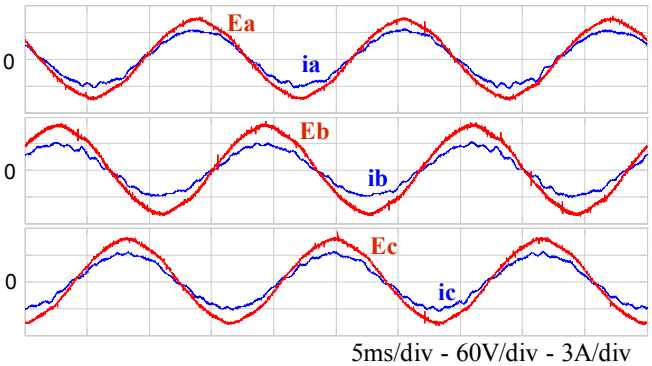

Fig.18 Line to neutral grid voltages and line currents (E_a,i_a), (E_b,i_b), and (E_c, i_c) obtained under 10% decrease of E_a and 5% of E_c .

This article has been accepted for publication in a future issue of this journal, but has not been fully edited. Content may change prior to final publication. Citation information: DOI 10.1109/TPEL.2015.2421480, IEEE Transactions on Power Electronics

This estimator, which operates downstream of the PIR control loop, allows the converter to provide balanced output voltages and consequently an almost constant active power free of low-frequency ripple supplied from the grid.

APPENDIX

According to (11.b), the expression of $I^+_{q\_ref}$ is :

$$I^+_{q\_ref} = I^+ \sin(\varphi^+_{ref}) \qquad (A1)$$

Moreover, the following relationships are derived from equation (10):

$$E^+ = E^+_d \qquad (A2)$$

$$(E^-)^2 = \left[(E_d - E^+_d)^2 + \left(E_q\right)^2\right] \qquad (A3)$$

Therefore, reporting (9.a), (A2), and (A3), into (A1) yields equation (12.a). On the other hand, according to (11.b), the expression of $I^-_{q\_ref}$ is :

$$I^-_{q\_ref} = I^- \sin(-2\omega_i t - \varphi^-) \qquad (A4)$$

Reporting (8.a) and (9.b) into (A4) yields:

$$I^-_{q\_ref} = \frac{E^-}{E^+} I^+ \sin\left(2\omega_i t + \theta^- + \varphi^+_{ref}\right) \qquad (A5)$$

Equation (A5) can also be rewritten as follows:

$$I^-_{q_{ref}} = \frac{1}{\underbrace{E^+}_{E^+_d}}\left[\overbrace{E^-\sin(2\omega_i t + \theta^-)}^{-E^-_q} \quad \overbrace{I^+ cos(\varphi^+_{ref})}^{I^+_d}\right] + \frac{1}{\underbrace{E^+}_{E^+_d}}\left[\overbrace{E^-\cos(2\omega_i + \theta^-)}^{E^-_d} \quad \overbrace{I^+ sin(\varphi^+_{ref})}^{I^+_{q_{ref}}}\right] \qquad (A6)$$

Equation (A6) is quite equivalent to (12b) given in section III/A.

REFERENCES

[1] M. Hamouda, H. F. Blanchette, and K. Al-Haddad, "Indirect Matrix Converters' Enhanced Commutation Method," *IEEE Trans. Indus. Electron.*, vol. 62, no. 2, pp. 671-679, Feb. 2015.

[2] J. Rodriguez, M. Rivera, J. W. Kolar, and P. W. Wheeler, "A Review of Control and Modulation Methods for Matrix Converters," *IEEE Trans. Ind. Electron.*, vol. 59, no. 1, pp. 58-70, Jan. 2012.

[3] C.Qi, X. Chen, and Y. Qiu, "Carrier-Based Randomized Pulse Position Modulation of an Indirect Matrix Converter for Attenuating the Harmonic Peaks," *IEEE Trans. Power. Electron*, vol. 28, no. 7, pp. 3539-3548, Jul. 2013.

[4] M. Hamouda, H. F. Blanchette, K. Al-Haddad, and F. Fnaiech, "An Efficient DSP-FPGA-Based Real-Time Implementation Method of SVM Algorithms for an Indirect Matrix Converter," *IEEE Trans. Indus. Electron.*, vol. 58, no. 11, pp. 5024-5031, Nov. 2011.

[5] X. Liu, P. C. Loh, P. Wang, F. Blaabjerg, Y. Tang, and E. A. Al-Ammar, "Distributed Generation Using Indirect Matrix Converter in Reverse Power Mode," *IEEE Trans. Power Electron.*, vol. 28, no. 3, pp. 1072-1082, Mar. 2013.

[6] X. Liu, P. C. Loh, P. Wang, and F. Blaabjerg, "A Direct Power Conversion Topology for Grid Integration of Hybrid AC/DC Energy Resources," *IEEE Trans. Indus. Electron.*, vol. 60, no. 12, pp. 5696-5707, Dec. 2013.

[7] T. D. Nguyen, and H.H. Lee., "Dual Three-Phase Indirect Matrix Converter With Carrier-Based PWM Method," *IEEE Trans. Power Electron.*, vol. 2, no. 29, pp. 569-581, Feb 2014.

[8] R. Peña, R. Cárdenas, E. Reyes, J. Clare, and P. Wheeler, "Control of a Doubly Fed Induction Generator via an Indirect Matrix Converter With Changing DC Voltage," *IEEE Trans. Indus.Electron.*, vol. 58, no. 10, pp. 4554-4674, Oct. 2011.

[9] S.S. Sebtahmadi, H. Pirasteh, S.H.A. Kaboli, A. Radan, and S. Mekhleif, "A 12-Sector Space Vector Switching Scheme for Performance Improvement of Matrix-Converter-Based DTC of IM Drive," *IEEE Trans. Power Electron*, vol. 30, no. 07, pp. 3804 - 3817, Jul. 2015.

[10] H. Hojabri, H. Mokhtari, and L. Chang, "Reactive Power Control of Permanent-Magnet Synchronous Wind Generator With Matrix Converter," *IEEE Trans. Power Deliv.*, vol. 28, no. 2, pp. 575-584, Apr 2013.

[11] J. Monteiro, J. F. Silva, S. F. Pinto, and J. Palma, "Linear and Sliding-Mode Control Design for Matrix Converter-Based Unified Power Flow Controllers," *IEEE. Trans. Power Electron.*, vol. 29, no. 7, pp. 3357-3367, Jul. 2014.

[12] D. Casadei, G. Serra, and A. Tani, "A General Approach for the Analysis of the Input Power Quality in Matrix Converters," *IEEE Trans. Power Electron*, vol. 13, no. 5, pp. 852-891, Sep. 1998.

[13] H. M. Nguyen, H.H. Lee, and T.W Chun, "Input Power Factor Compensation Algorithms Using a New Direct-SVM Method for Matrix Converter," *IEEE Trans. Ind. Electron.*, vol. 58, no. 1, pp. 232-243, Jan. 2011.

[14] A. K. Sahoo, K. Basu, and N. Mohan, "Systematic Input Filter Design of Matrix Converter by Analytical Estimation of RMS Current Ripple," *IEEE Trans. Indus. Electron.*, vol. 62, no. 1, pp. 132 - 143, Jan. 2015.

[15] K. You, D. Xiao, M. F. Rahman, and M. N. Uddin, "Applying Reduced General Direct Space Vector Modulation Approach of AC–AC Matrix Converter Theory to Achieve Direct Power Factor Controlled Three-Phase AC–DC Matrix Rectifier," *IEEE Trans. Ind. Appl.*, vol. 50, no. 3, pp. 2243-2257, May/Jun. 2014.

[16] M. Hamouda, F. Fnaiech, and K. AL-Haddad, "Input filter design for SVM Dual-Bridge Matrix Converters," in *IEEE ISIE*, Montréal, Canada, 2006, pp. 797-802.

[17] M. Hamouda, F. Fnaiech, and K. Al-Haddad, "Control of the reactive line current provided by a Dual-Bridge Matrix Converter using the input-output feedback linearization approach," in *IEEE ISIE*, Montréal, Canada, 2006, pp. 803-808.

[18] IEEE standard definitions for the measurement of electric power quantities under sinusoidal, nonsinusoidal, balanced, or unbalanced conditions, IEEE Stdandards 1459-2010, , pp. 1-40, Mar. 2010.

[19] A. Camacho, M. Castilla, J. Miret, R. Guzman, and A. Borrell, "Reactive Power Control for Distributed Generation Power Plants to Comply with Voltage Limits During Grid Faults," *IEEE Trans. Power Electron.*, vol. 29, no. 11, pp. 6224-6234, Nov. 2014.

[20] K. Ma, W. Chen, M. Liserre, and F. Blaabjerg, "Power controllability of three-phase converter with unbalanced AC source," *IEEE Trans. Power Electron.*, vol. 30, no. 3, pp. 1591-1604, Mar. 2015.

[21] M. Rivera, J. Rodriguez, J.R. Espinoza, and H. Abu-Rub, "Instantaneous Reactive Power Minimization and Current Control for an Indirect Matrix Converter Under a Distorted AC Supply," *IEEE Trans. Indus. Info.*, vol. 8, no. 3, pp. 482-490, Aug 2012.

[22] F. Blaabjerg, D. Casadei, C. Klumpner, and M. Matteini, "Comparison of Two Current Modulation Strategies for Matrix Converters Under Unbalanced Input Voltage Conditions," *IEEE Trans. Ind. Electron.*, vol. 49, no. 2, pp. 289-296, Apr. 2002.

[23] T. Satish, K.K. Mohapatra, and N. Mohan, "Modulation Methods Based on a Novel Carried-Based PWM Scheme for Matrix Converter Operation under Unbalanced Input Voltages," in *APEC '06. Twenty-First Annual IEEE* , 19-23 March, 2006, pp. 127-132.

[24] Y. Yan, H. An, T. Shi, and C. Xia, "Improved double line voltage synthesis of matrix converter for input current enhancement under unbalanced power supply," *IET Power Electron.*, vol. 6, no. 4, pp. 798-808, Jul. 2013.

[25] J. K. Kang, H. Hara, A. M. Hava, E. Yamamoto, E. Watanabe, and T. J. Kume, "The matrix converter drive performance under abnormal input voltage conditions," *IEEE Trans. Power Electron.*, vol. 17, no. 5, pp. 721–730, Sep. 2002.

[26] X. Wang, H. Lin, H. She, and B. Feng, "A Research on Space Vector Modulation Strategy for Matrix Converter Under Abnormal Input-Voltage Conditions," *IEEE Trans. Ind. Electron.*, vol. 59, no. 1, pp. 93-104, Jan. 2012.

[27] X. Li, M. Su, Y. Sun, H. Dan, and W. Xiong, "Modulation strategies based on mathematical construction method for matrix converter under

This article has been accepted for publication in a future issue of this journal, but has not been fully edited. Content may change prior to final publication. Citation information: DOI 10.1109/TPEL.2015.2421480, IEEE Transactions on Power Electronics

unbalanced input voltages," *IET Power Electron.*, vol. 6, no. 3, pp. 434-445, Jun. 2013.
[28]L. Wei, Y. Matsushita, and T.A. Lipo, "Investigation of dual-bridge matrix converter operation under unbalanced source voltages," in *IEEE PESC*, 2003, pp. 1293-1298.
[29]C. Klumpner, T. Wijekoon, and P. Wheeler, "Active Compensation of Unbalanced Supply Voltage for Two-Stage Direct Power Converters Using the Clamp Capacitor," in *IEEE PESC*, Recife, 2005, pp. 2376 - 2382.
[30]P. Nielsen, F. Blaabjerg, and J. K. Pedersen, "Space vector modulated matrix converter with minimized number of switching and feedforward compensation of input voltage unbalance," in *PEDES*, New Delhi, 1996, pp. 833-839.
[31]R. Vargas, J. Rodríguez, U. Ammann, and. P. W. Wheeler, "Predictive Current Control of an Induction Machine Fed by a Matrix Converter With Reactive Power Control," *IEEE Trans. Ind. Electron.*, vol. 55, no. 12, pp. 4362-4371, Dec. 2008.
[32]M. Hamouda, K. Al-Haddad, F. Fnaiech, and H.F Blanchette, "Input-state feedback linearization control of two-stage matrix converters interfaced with high-speed microturbine generators," in *Proc. IEEE EPC*, Canada, 2007, pp. 302-307.
[33]I. Sato, J-I. Itoh, H. Ohguchi, A. Odaka, and H. Mine, "An Improvement Method of Matrix Converter Drives Under Input Voltage Disturbances," *IEEE Trans. Power Electron.*, vol. 22, no. 1, pp. 132-138, Jan. 2007.
[34]D. Roiu, R.I. Bojoi,L. Rodrigues, and A. Tenconi, "New Stationary Frame Control Scheme for Three-Phase PWM Rectifiers Under Unbalanced Voltage Dips Conditions," *IEEE Trans. Indus. App.*, vol. 46, no. 1, pp. 268-277, Jan/Feb. 2010.
[35]M. Reyes, P. Rodriguez, S. Vazquez, A. Luna, R. Teodorescu, and J. M. Carrasco, "Enhanced Decoupled Double Synchronous Reference Frame Current Controller for Unbalanced Grid-Voltage Conditions," *IEEE Trans. Power Electron.*, vol. 27, no. 9, pp. 3934-3943, Sep. 2012.
[36]D. Casadei, G. Serra, and A. Tani, "Reduction of the input current harmonic content in matrix converters under input output unbalance," *IEEE Trans. Indus. Electron.*, vol. 45, no. 3, pp. 401–410, Jun. 1998.
[37]Y.Suh, and T.A.Lipo, "Modeling and Analysis of Instantaneous Active and Reactive Power for PWM AC/DC Converter Under Generalized Unbalanced Network," *IEEE Tans. Power. Del.*, vol. 21, no. 3, pp. 1530-1540, Jul. 2006.
[38]M. Hamouda, F. Fnaiech, and K. AL-Haddad, "Modeling and adaptive control of Two-Stage Matrix Converters," *International Review of Electrical Engineering*, vol. 3, no. 1, pp. 83-92, Jan 2008.
[39]M.F. Iacchetti, G.D. Marques, and R. Perini, "Torque Ripple Reduction in a DFIG-DC System by Resonant Current Controllers," *IEEE Trans. Power Electron*, vol. 30, no. 8, pp. 4244 - 4254, Aug. 2015.
[40]A.G. Yepes, F.D. freijedo, O. Lopez, J. Doval-Gandoy, "High-Performance Digital Resonant Controllers Implemented With Two Integrators," *IEEE Trans. Power. Electron*, vol. 26, no. 2, pp. 563-576, Feb 2011.
[41]J.Hu, Y. He, L. Xu, B.W. Williams, "Improved Control of DFIG Systems During Network Unbalance using PI-R Current Regulators," *IEEE Trans. Indus. Electron.*, vol. 56, no. 2, pp. 439-451, Feb 2009.
[42]A. Vidal, F. D. Freijedo, A. G. Yepes, P. Fernandez-Comesana, J. Malvar, O. Lopez, J. Doval-Gandoy, "Assessment and Optimization of the Transient Response of Proportional-Resonant Current Controllers for Distributed Power Generation Systems," *IEEE Trans. Indus. Electron*, vol. 60, no. 4, pp. 1367-1383, Apr 2013.
[43]A. G. Yepes, F. D. Freijedo, J. Doval-Gandoy, O. Lopez, J. Malvar, P. Fernandez-Comesana, "Effect of Discretization Methods on the Performance of Resonant Controllers," *IEEE Trans. Power. Electron*, vol. 25, no. 7, pp. 1692-1712, Jul 2010.
[44]C. Garcia, M. Rivera, M. Lopez, J. Rodriguez, R. Pena, P. Wheeler, and R. Espinoza, "A Simple Current Control Strategy for a Four-Leg Indirect Matrix Converter," *IEEE. Trans. Power Electron.*, vol. 30, no. 04, pp. 2275-2283, Apr 2015.
[45]X. Guo, W. Liu, X. Zhang, X. Sun, Z. Lu, and J. M. Guerrero, "Flexible Control Strategy for Grid-Connected Inverter Under Unbalanced Grid Faults Without PLL," *IEEE Trans. Power Electron.*, vol. 30, no. 4, pp. 1773-1778, Apr. 2015.

Mahmoud Hamouda received the B.S., Agregation, M.S., and Ph.D. degrees in electrical engineering from ENSET and the Ecole Superieure des Sciences et Techniques, University of Tunis, Tunisia, in 1995, 1996, 2004, and 2010 respectively. He is presently an Associate Professor of electrical engineering with ISSAT of Sousse, University of Sousse, Tunisia. He is affiliated with Canada Research Chair in Electric Energy Conversion and Power Electronics, "CRC-EECPE", Ecole de Technologie Supérieure (ETS), Montreal, Canada. He is also a member of the research unit SAGE, ENISO, University of Sousse, Tunisia.
His main research interests include renewable energy conversion systems, DsP and FPGA for embedded real time control, unbalanced weak grid systems, development of advanced controllers such as nonlinear control of matrix, multilevel, multicellular, multiphase converters, and grid-tied converters.

Handy Fortin Blanchette (S'07–M'10) received the B.Eng.,M.Eng., and Ph.D. degrees in electrical engineering from École de Technologie Supérieure (ETS), Montreal, PQ, Canada, in 2001, 2003, and 2010, respectively.
From 1994 to 1997, he was engaged in industrial automation. From 1998 to 2000, he was with the Bombardier Transport-ETS Research Laboratory, Montreal, where he worked on a high power traction system. From 2001 to 2003, he was involved in the development of an electrical drive library for the Simulink (MATLAB) environment. From 2007 to 2010, he was with OPAL-RT Technologies, where he led CPU- and FPGA-based power electronics real-time simulation projects. From 2010 to 2011, he was a Visiting Scholar with the Center for Power Electronic and System, Virginia Polytechnic Institute and State University, Blacksburg, where he was involved in the packaging of high-temperature converters for aircraft applications. He is presently an Associate Professor of electrical engineering with Ecole de Technologie Supérieure, Montreal. His current research interests include EMI prediction, circuit modeling, and high density power converter packaging.

Kamal Al-Haddad (S'82–M'88–SM'92–F'07) received the B.Sc.A. and M.Sc.A. degrees from the University of Québec à Trois-Rivières, Canada, in 1982 and 1984, respectively, and the Ph.D. degree from the Institut National Polythechnique, Toulouse, France, in 1988.
Since June 1990, he has been a Professor with the Electrical Engineering Department, École de Technologie Supérieure (ETS), Montreal, QC, where he has been the holder of the Canada Research Chair in Electric Energy Conversion and Power Electronics since 2002. He has supervised more than 100 Ph.D. and M.Sc.A. students working in the field of power electronics. He is a Consultant and has established very solid link with many Canadian industries working in the field of power electronics, electric transportation, aeronautics, and telecommunications. He has coauthored more than 500 transactions and conference papers. His fields of interest are in high efficient static power converters, harmonics and reactive power control using hybrid filters, switch mode and resonant converters including the modeling, control, and development of prototypes for various industrial applications in electric traction, electrification and transportation, renewable energy, microgrids, power supplies for drives, telecommunication, etc.
Prof. Al-Haddad is a fellow member of the Canadian Academy of Engineering. He is IEEE IES President Elect, Associate editor of the Transactions on Industrial Informatics and IES Distinguished Lecturer.